Experiments in Fluids 23 (1997) 130–140

Fundamentals of a liquid (soap) film tunnel

M. Beizaie, M. Gharib

Abstract The continuously running liquid film tunnel (LFT) is a novel device suitable for the study of two-dimensional flows. In this innovation, the films start from a reservoir, run over a horizontal or non-horizontal wire frame and get pulled/washed by a water sheet or by gravity of liquid film. However, despite the simple design and widespread application of LFT, its working mechanisms are not well understood. In the present work, an experimental effort for explaining these mechanisms is reported. The results show that both film velocities and film flow rates increase with water sheet velocity up to a saturation level. This behavior is described via a force balance between the shear force produced by the water sheet and the opposing pulling force of reservoir and boundary layer frictions. The results also show that the average film thickness depends on the surfactant concentration. This is as predicted by a model based on Langmuir's adsorption theory, in which the liquid film contains two external monolayers of surfactant and a slab of surfactant solution in between. When a film is drawn from the reservoir to the water sheet, the surfactant molecules start migrating from the former to the latter. To restore the thermodynamic equilibrium, the dragged film pulls more surfactant due to Marangoni elasticity, and thus a flow is established. The film flow soon reaches an equilibrium rate as required by the force balance mentioned above.

List of symbols

A	area
b	width
C	concentration of surfactant
d	diameter of a cylinder; thickness of a liquid film
D	drag force
E	elasticity modulus
f	shedding frequency
F	force
K	a constant [see Eq. (7)]
L	length
P	pressure
q	volumetric flow rate
R	gas law constant
Re	Reynolds number (density) (velocity) (characteristic length)/viscosity
St	Strouhal number (shedding frequency) (characteristic length)/velocity
T	temperature
V	velocity
W	weight
x, y, z	Cartesian coordinates
Γ	hypothetical two-dimensional concentration of the surfactant at surface
μ	viscosity
θ	film's angle with gravitational direction
ρ	density
σ	surface tension
τ	shear stress

Subscripts

1	surfactant first point
2	second point
∞	saturation value
a	air's boundary layer; sound
b	ribbon's boundary layer
c	critical
d	cylinder
f	liquid film
G	Gibbs
M	Marangoni
o	initial value
r	reservoir
w	water sheet

Received: *15 August 1996*/*Accepted*: *12 November 1996*

M. Beizaie
Department of AMES, University of California, San Diego,
9500 Gilman Drive, La Jolla, CA 92093, USA

M. Gharib
Graduate Aeronautical Laboratory,
California Institute of Technology, 1200 California Boulevard,
Pasadena, CA 91125, USA

Correspondence to: M. Gharib

This work was supported by a grant from the National Science Foundation (NSF Contract MSM 88-20182). Both authors would like to thank Professor Mysels for his enthusiastic support of soap-film efforts in our group.

1 Introduction

Theoretical and experimental studies of two-dimensional flows are central to the issue of large vortical motion, transition and turbulence in geostrophic flows. A common characteristic of atmospheric or oceanic flows is their large surface areas as

compared to depth, which makes them difficult to simulate in the laboratory. A literature survey would reveal that the theoretical side of such studies has been given much more attention than the experimental side, since the latter can rarely simulate the former precisely. Another problem in simulating two-dimensional flows in the laboratory is due to the difficulty of isolating two-dimensional flows from the evolving three-dimensional instabilities.

Liquid films, especially those made out of surfactant solutions have long been nominated as good media for the production and study of two-dimensional hydrodynamics (Mysels et al. 1959; Frankel and Mysels 1969; Mysels and Frankel 1978; Rusanov and Krotov 1979; Couder 1981; Couder et al. 1989). These films; usually called soap films, although a surfactant is not necessarily a soap; are very thin, self-sustained fluid layers in which hydrodynamical experiments can be done. In such a film, the velocity field is confined to its surface and is practically two-dimensional. As was suggested ingeniously by Mysels and demonstrated in excellent series of experiments by Couder, soap films are good candidates for the simulation of 2-dimensional flows. However, since soap films age with time, the experiments that involve still films suffer from several shortcomings. The observation periods are short and the films do not maintain a uniform mean thickness with time, which makes quantitative flow measurements difficult.

In an effort to avoid such shortcomings, a continuously running liquid film tunnel (LFT) was invented in 1987 by Gharib and Derango (1987, 1989), and used by us to study a variety of two-dimensional flows (Gharib and Beizaie 1989, 1990, 1992; Gharib 1993; Beizaie 1991). This LFT, which has undergone considerable improvement since its invention, is described in the next section.

2
Liquid film tunnel: concept

The Liquid Film Tunnel consists of a wire frame one end of which is positioned in a diluted surfactant mixture while the other end is subjected to either of two film-pulling mechanisms (Fig. 1). The frame is constructed of 1/8″ rods of either copper or steel.

The main portion of the LFT is a horizontal frame section consisting of two parallel rods (Fig. 1a). This flat section is supported by two legs, one at each end. The liquid films are pulled by the shearing action of a two-dimensional water jet which is produced by flow of water through a rectangular opening, mounted on a horizontal pipe. By rotating this pipe, the shearing angle can be changed and by varying the water flow rate one can vary the pulling force. Note that the leg at the film/water jet interface has fork-like structures. These structures help to stabilize the film/water jet interface.

The size of the frame is limited by the horizontal film's tendency to bow at the flat section of the tunnel. The maximum width of the frame to avoid this effect is 4″. In the horizontal version of LFT, the streamwise length of the horizontal test section can be extended up to 1.5 ft without greatly reducing the life of the film. Several other factors, including dry air, severe ventilation, vibration and unsteadiness or turbulence in the water jet can shorten the film life. Fine cloth ribbons are glued to the top of the frame to help prevent rupture of the liquid films due to water evaporation. So, the films are actually supported by these thin wet ribbons rather than by the rods themselves. Therefore, the menisci along the ribbons have a constant thickness, independent of the surfactant concentration. The horizontal films are also quite uniform in thickness when running steadily, but this thickness can be changed by changing the surfactant concentration. With a steady water jet in the horizontal version, and in the absence of severe ventilation and vibration, the films can run for hours, provided that a fresh surfactant mixture is added continuously to the reservoir.

Liquid films can be visualized through light interference effects produced by small variations in the film thickness. Such variations are produced during pulling of the film from the reservoir due to gravitational effects. By optical techniques (Isenberg 1978), the maximum film thickness variation between two consecutive fringe patterns can be calculated as (wavelength)/[2(refraction index)(cosine of refraction angle)]. For a typical horizontal film, this is estimated to be in the order of 100 nm for a 5 μm thick film lit by monochromatic green light of 500 nm wavelength. Usually, the distance between such fringes in the horizontal section is about 5–10 cm. Therefore, the horizontal section of the film is uniform in thickness by an error less than 0.0002%. Figure 2 represents a typical thickness visualization for the horizontal films.

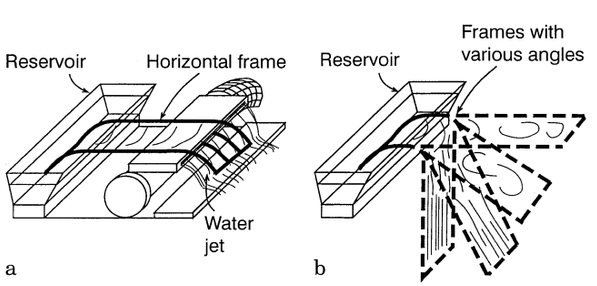

Fig. 1a, b. The liquid film tunnel (LFT). **a** Driven by a running water sheet; **b** gravity; the thicklines represent the fine cloth ribbons glued on top of the frames

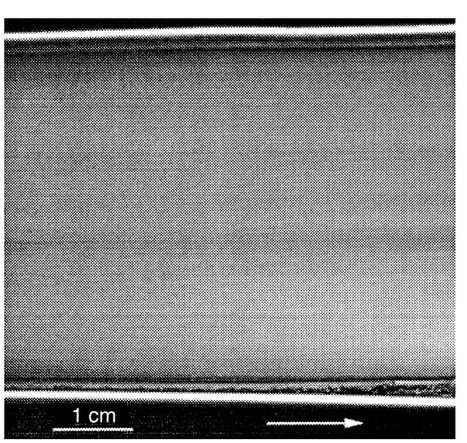

Fig. 2. Typical film thickness visualization for conditions **a** and **b** in Fig. 1, depicting the thickness uniformity by the absence of fringe patterns

A second version of LFT was studied, with the frame continuing to form a non-horizontal section in which the liquid film moves under gravity and thus pulls the liquid film (Fig. 1b). In this case, there is no need for a water jet as a pulling mechanism; however, a combination of the two mechanisms is possible also.

Liquid films in the non-horizontal (angle with horizon greater than 45°) section are far from being uniform in thickness. Indeed, we have estimated a sharp change of thickness from several hundred microns at the meniscus to a few microns at the center. This means there is a thickness gradient of several hundred microns over a few centimeters of film width, i.e. of the order of 1%. We concluded that the vertical section cannot serve as an LFT in two-dimensional flows which need uniform film thickness.

In our experiments, we also tried a totally vertical frame with the surfactant solution running over it, as shown in Fig. 3a. Although this appeared like a fast running LFT, close examinations revealed the existence of extremely large-scale non-uniformities in the background flow and thickness (similar to the second version with angle greater than 45°); see Fig. 3b. Since we could not improve the flow conditions for non-horizontal cases, we did not continue this line of experiments. However, a group at the University of Pittsburgh has recently reported some success with application of vertical liquid films.

The liquid film tunnel is started by pulling a film from the reservoir's surface and drawing it on the wet frame by a wet cloth and finally contacting the film to the end of the frame; that is, contacting to the running water sheet in the first version, or to the end of the frame in the second. Once a film starts to run, it produces two-dimensional patterns depending on the frame's design. Some examples include frames that produce jets, cavity flow, grid turbulence and vortex shedding (Gharib and Derango 1989). The patterns are visible due to the light interference effects produced by small variations in the film thickness.

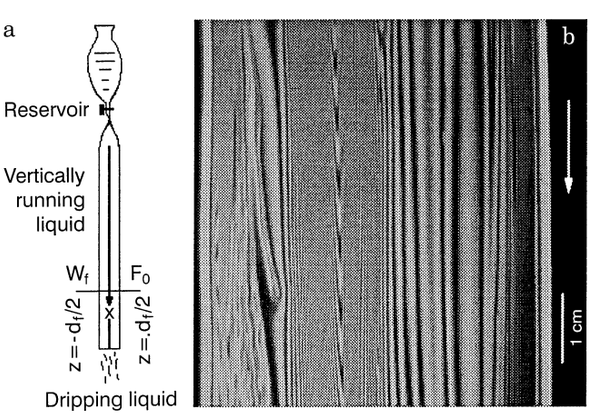

Fig. 3a, b. Flow in a totally vertical frame. **a** Schematic; **b** photograph; flow visualization depicts extreme thickness non-uniformity through existence of dense fringe patterns

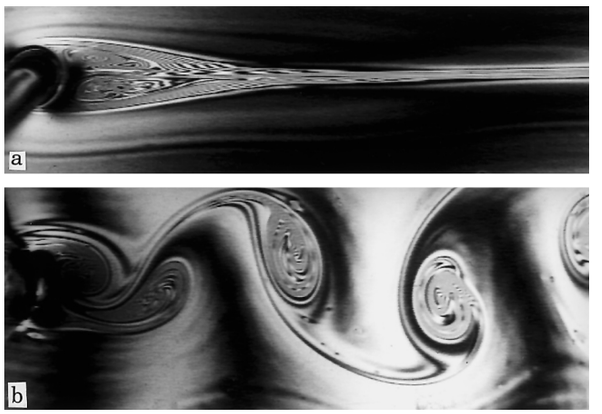

Fig. 4a, b. Two-dimensional wake; **a** $Re \cong 25$, steady wake; **b** $Re \cong 100$, Karman vortex street

Fig. 5. Two-dimensional jet; $Re \cong 500$; visualization through color interference technique

3
Examples of the generated flows

By piercing the film surface with a small cylinder, one can generate a two-dimensional wake pattern. Figure 4 shows examples of such wake flows for two different Reynolds numbers. Figure 5 is a color photograph of a two-dimensional jet produced by two converging bars in the film; the jet's Reynolds number is about 500. Figure 6 is monochromatic picture of two-dimensional grid turbulence in a 4 cm wide liquid film. The film was produced by a 0.5% surfactant mixture and run at about 30 cm/s through an array of 1.4 mm dia. rods spaced 3.2 mm center to center. The undisturbed film thickness was estimated to be about 7 μm.

4
Hydrodynamics of LFT

Given the virtual complexity of the surfactant (soap) films, it is not surprising that the operational mechanisms of the LFT,

Fig. 6. Two-dimensional grid turbulence based on grid spacing Reynolds number of 110

with such a simple design and unsuccessful application have not been fully understood, which left the LFT improvements to develop largely through trial and error. For example, for some time the humidity of the surrounding air was thought to be an important factor regarding the life span of the films. Keeping the frames wet by a variety of techniques finally led to the idea of gluing thin cloth ribbons on their top surfaces. This method increased the films' life span quite impressively, regardless of the air humidity. As another example, maintaining a constant level of surfactant solution in the reservoir was known to be important for obvious reasons, but the optimum level was found to be dependent on both the frame's design and the surfactant concentration.

The purpose of this section is to describe the fundamental physics underlying operation of LFT. To do this, it is crucial to have an accurate description of the forces involved with the motion of liquid films. It is thus important to evaluate the source and nature of a pulling force generated at the liquid film/water sheet contact (or the vertical film section) and the resistive forces opposing it. A correct force balance, in turn, needs a thorough understanding of the liquid film itself. Therefore, a reliable model for the liquid film is also essential.

The liquid film model presented here is based on the observations of the LFT and the works of several researchers, notably, Mysels (Mysels et al. 1959, 1969, 1978) and Couder (Couder et al. 1989). In this model, a liquid film consists of two nanometer-thick monolayers of surfactant molecules and a thin (a few microns) slab of surfactant solution between them. Except to the neighborhoods of the reservoir and the water sheet, horizontal liquid film running at steady state is substantially uniform in thickness. Also, since the surfactant monolayers and the thin intermediate slab are thought to be rigidified (Mysels and Frankel 1978), it is assumed that the three layers of a film move together (similar to the motion of a tough belt on a pulley). This implies that the film's thickness does not depend on its hydrodynamics; rather, it is determined by the slow cross-sectional thermodynamic processes. In other words, the surfactant molecules have enough time for diffusion from the intermediate slab to either surface. Since mass diffusivity of surfactants in water is of the order of 10^{-6} cm^2/s, the time scale for this process, i.e. (film thickness)^2/diffusivity, is of the order of 0.01 s for a film one micron thick, so this should be due to the Gibbs elasticity of the film (Couder et al. 1989). In practice, however, the presence of impurities makes the equilibrium more difficult to reach (Rusanov and Krotov 1979), so that Marangoni elasticity can be observed up to times of the order of a second (Couder et al. 1989).

On the other hand, local disturbances such as vortices lead to local changes in the liquid film's thickness. This is thought to be due to the cross-sectional movement of the interstitial layer due to the compressibility of liquid film (Couder et al. 1989). In other words, the middle layer is sucked in or squeezed out locally by the local movement of the two outer layers. This mechanism, too, is governed by the Marangoni elasticity.

The work reported here is mainly experimental in nature, but theoretical models for the liquid film and the LFT are employed for analysing the obtained results. In Sect. 4.1, it is shown that the LFT flows exhibit a Newtonian behavior. A model liquid film is presented in Sect. 4.2, and the force balance for the LFT is described in Sect. 4.3.

4.1
Determination of the type of flow

Because of the role of surfactants in the motion of the liquid film, an examination of the type of the flow is required. Gharib and Derango (1989) showed that the dynamics of film motion are similar to those observed in three-dimensional Newtonian flows. To prove this point, they employed the vortex shedding behind a circular cylinder and an empirical relationship suggested by Roshko (1953), i.e. $St = f d_d / V_f = 0.212 - 0.45/Re$, where St is the Strouhal number, f is the shedding frequency, d_d is the cylinder diameter, V_f is the free stream velocity and Re is the Reynolds number.

Figure 7 was constructed by measuring the velocity and frequency of sheddings behind cylinders of known size in

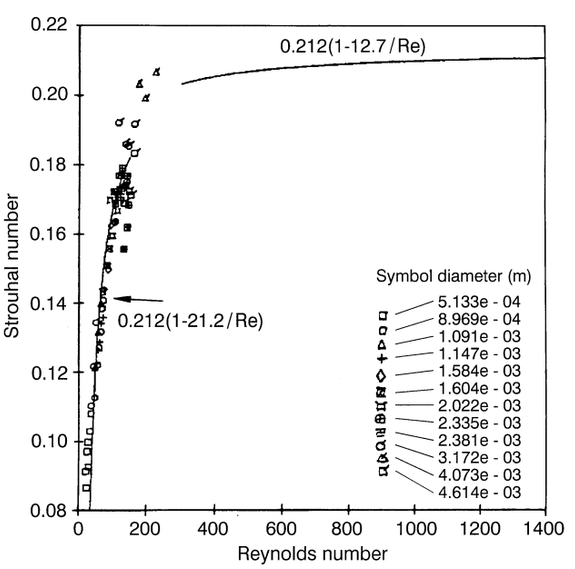

Fig. 7. Strouhal number–Reynolds number relation for various circular cylinder wakes in the LFT (from Gharib and Derango 1989)

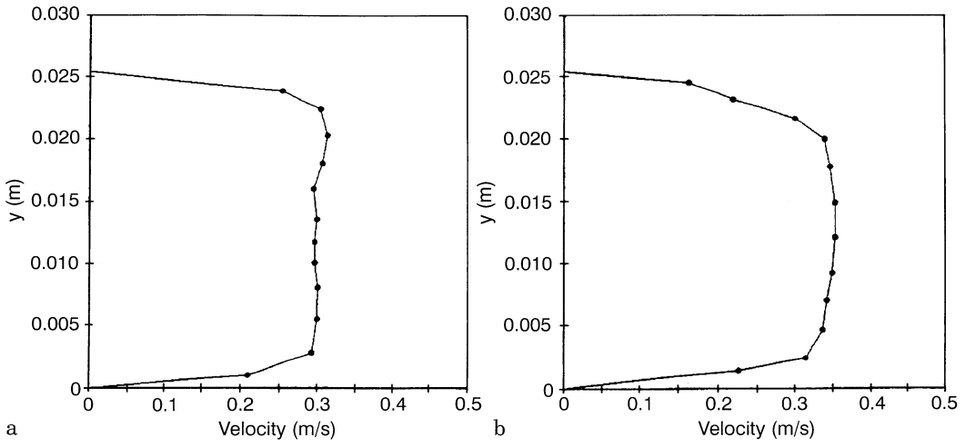

Fig. 8a, b. Mean velocity profile **a** 4 cm from test section entrance; **b** at 10 cm position showing development of boundary layers on the side walls (from Gharib and Derango 1989)

the film and then using the Strouhal number to obtain the Reynolds number and consequently the film viscosity from Roshko's equation. The assumption was that if this viscosity is a true representation of the film viscosity, then by using the empirically determined film viscosity, one should be able to construct Roshko's curve for the two-dimensional vortex shedding process in the liquid film tunnel. This figure shows that a two-dimensional vortex shedding process at a macroscopic level is strongly similar to its three-dimensional counterpart. It also shows that vortex sheddings can be used as a practical means of estimating film viscosities, as done at point identified by an arrow (3.75 cP). Note that his estimated film viscosity includes the effect of all the experimental factors, such as the meniscus formation around the cylinder.

The free stream velocity across the test section, V_f, was measured by a laser Doppler velocimeter. The results at two streamwise positions are shown in Fig. 8.

4.2
Theoretical model for the liquid film

A schematic diagram for a test section of the LFT is shown in Fig. 9. This is for a horizontal film running on a plain frame at a steady state.

Since the films are typically a few microns thick, running at 5–30 cm/s, and diffusivity of surfactants is relatively small, it is reasonable to assume that the concentrations vary in the z-direction only. Note that the film is not shown to scale, since the surfactant molecules have a size order of a nanometer only.

The migration of a surfactant molecule to/from either surface and the interstitial zone is governed by its chemical potential, which is the partial derivative of the system's Gibbs free energy with respect to the number of moles of the surfactant, while other numbers of moles, temperature and pressure are all kept constant. Thus, the hypothetical two-dimensional surfactant concentration at either surface of the film, Γ_1, is related to the three-dimensional concentration C_f in the bulk of the film. This relationship has been studied by Rusanov and Krotov (1979) for stationary films of sodium dodecyl sulfate aqueous solutions.

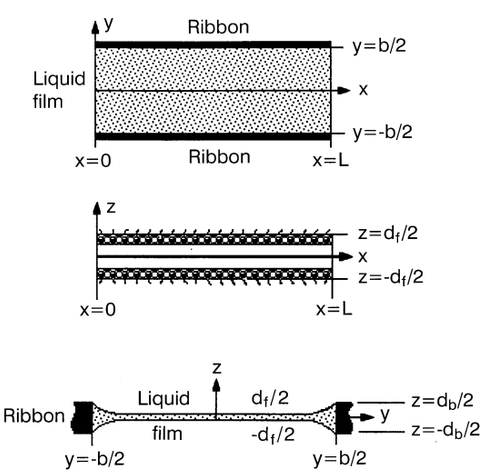

Fig. 9. The test section of the LFT (not to scale)

Unfortunately, no such study is available yet for moving films, but one still can rely on the fact that the population of surfactant molecules at the free surface is always much more than in the bulk. The reason for this reliance is the chemical nature of the surfactants, i.e. their consistence of a hydrophilic polar head and a hydrophobic hydrocarbon tail. These tails always tend to avoid water molecules and hence the surfactant molecules accumulate on the free surfaces ($z = \pm d_f/2$) with their tails in the air. Under steady-state conditions, it is conceivable that the two surfactant films and the interstitial layer are at equilibrium. In other words, the molecular forces resulting from the different chemical potentials counteract in such a way that a uniform film thickness is established.

Observation of a running liquid film at its onset over the reservoir shows that it is the surface layer of the liquid (reservoir's contents) that is being pulled out, bisected at the Plateau border and transformed to a sandwich attached to the frame. Therefore, it is reasonable to assume Γ_1 to be the same

as for the surface layer of the liquid in the reservoir. On the other hand, a mass balance over the control volume of Fig. 9 ($0<x<L$; $-b/2<y<b/2$; $-d_f/2<z<d_f/2$) dictates that C_f should be less than $C_{1,r}$, the surfactant concentration in the bulk of the reservoir's contents, because of the conservation of mass:

total number of surfactant molecules $= Lbd_f C_{1,f}$
number of surfactant molecules on the two surfaces $= 2Lb\Gamma_1$
number of surfactant molecules in the interstitial zone $= Lbd_f C_f$

$$Lbd_f C_{1,f} = 2Lb\Gamma_1 + Lbd_f C_f$$

$$C_{1,f} = C_f + (2\Gamma_1 / d_f) \tag{1}$$

where $C_{1,f}$ is the overall surfactant concentration in the film. In other words, $C_{1,f}$ is the number of surfactant molecules present in a unit volume of the liquid film.

In practice, however, $C_{1,r} = C_{1,f}$, since the film's volume is much smaller than that of the liquid in the reservoir.

The equation of state of surfactant molecules, as adopted by Szyszkowski based on Langmuir's adsorption theory, at temperature T and atmospheric pressure is (Rusanov and Krotov 1979)

$$\sigma - \sigma_o = RT\Gamma_{1,\infty} \ln\left(1 - \frac{\Gamma_1}{\Gamma_{1,\infty}}\right) \tag{2}$$

The right-hand side of Eq. (2) is called the spreading pressure of the surfactant. By series expansion for the dilute solutions ($\Gamma_1 \ll \Gamma_{1,\infty}$), one obtains

$$\sigma_o - \sigma = RT\Gamma_1 \tag{3}$$

which is similar to a two-dimensional perfect gas law.

Following the procedure adopted for stationary films by Couder et al. (1989), the Gibbs elasticity modulus of a moving film may be defined by

$$E_G = \frac{2\mathrm{d}\sigma}{\mathrm{d}(\ln A)} = \frac{-2A\,\mathrm{d}\sigma}{\mathrm{d}A} \tag{4}$$

where A is the surface area of the film. Note that while the film is confined to fixed boundaries as shown in Fig. 2, E_G is virtually always non-zero because $\mathrm{d}\sigma/\mathrm{d}A$ can never be zero.

The Marangoni elasticity modulus may similarly be defined for dilute solutions:

$$E_M = 2RT\Gamma_1 \tag{5}$$

The speed of sound in the film, V_a, is given as (Couder et al. 1989)

$$V_a = (2E/\rho_f d_f)^{1/2} \tag{6}$$

where E is E_G or E_M depending on the time scale of the disturbance. Following Couder et al., $E = E_M \cong 0.088$ N/m for the present work. Thus, $V_a \cong 3$ m/s in a 10 mm-thick film and $V_a \cong 9.4$ m/s when $d_f = 1\,\mu$m.

If a linear relation exists between Γ_1 and C_f as shown by Rusanov and Krotov (1979) for stationary films, then after substituting C_f with Γ_1/K, Eq. (1) becomes

$$\Gamma_1 = C_{1,f} d_f K/(d_f + 2K) \tag{7}$$

Using this in Eqs. (3) and (4), then assuming $A/d_f =$ constant (constant film volume) one finds

$$\begin{aligned} E_G &= -2d_f \mathrm{d}\sigma/\mathrm{d}(d_f) \\ &= 2RTd_f\,\mathrm{d}\Gamma_1/\mathrm{d}(d_f) \\ &= 4RTC_{1,f}\,d_f K^2/(d_f + 2K)^2 \end{aligned} \tag{8}$$

In the limit of thin films ($d_f \ll 2K$), $E_G \cong E_M$ because the interstitial fluid is too thin to provide surfactant molecules to either surface. These thin films can be only a few nanometers thick (Couder et al. 1989).

4.3
A force balance for the LFT

The forces acting on a moving horizontal liquid film are sketched in Fig. 10.

When a horizontal film is considered, the film's weight, W_f, is supported by the ribbons (i.e. a reaction of $-W_f$). For the other cases, i.e. when the film has an angle θ with the gravitational direction, the weight component $W_f \cos\theta$ *helps* the film movement.

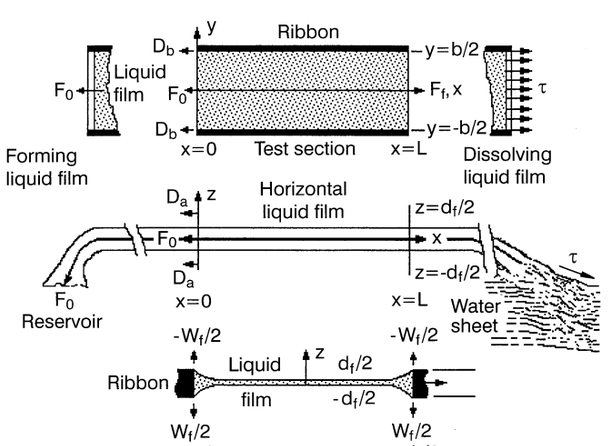

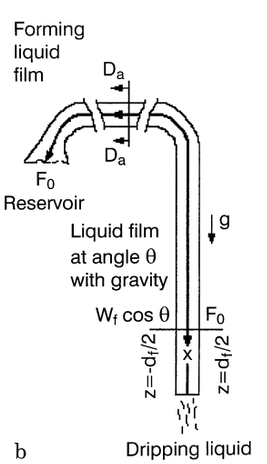

Fig. 10a, b. Force/stress schematics for the LFT (not to scale). **a** Driven by a running water sheet; **b** gravity

The air pressure P_a, is the same on both surfaces of the film, while the internal pressure P_f can vary with the film only in the neighborhoods of ribbons, the reservoir and the water sheet. Therefore, the pulling force F_f required to keep the film in steady motion should at least be balanced by the other forces shown in Fig. 10. They are, F_o, the reservoir's resistive pulling force and the boundary-layer friction forces D_a (film/air) and D_b (film/ribbon). For the steady-state case, a force balance for the LFT then becomes

$$F_f = F_o + 2D_a + 2D_b - W_f \cos\theta \tag{9}$$

The liquid film has to counter the friction forces of the boundary layers along the entire length of the frame, i.e. with air at $y = -b/2$ to $b/2$, $z = \pm d_f/2$ and the ribbons at $y = \pm b/2$, $z = -d_b/2$ to $d_b/2$. It also has to overcome the reservoir's resistive pulling force, F_o.

If the shear force generated at the contact with the water sheet is large enough, i.e. V_w is sufficiently large, a quasi-steady state is achieved in a rather short time, since the frame is only 30–40 cm long.

The mentioned shear stress is due to an interaction between perpetually vibrating surfactant molecules and the running water sheet. Because of the physical similarity in terms of molecular vibration, this shear stress can be estimated by a gas-kinetics dimensional analysis (Liepmann and Roshko 1957) and the speed of sound from Eq. (6):

$$\tau = \rho_f V_a V_w = V_w (2E\rho_f / d_f)^{1/2} \tag{10}$$

where ρ_f is the film's density, safely the same as that of the liquid in the reservoir.

The friction force (per unit length) in either liquid film/ribbon boundary layer, D_b, is assessed as follows (Schlichting 1968):

$$D_b = 0.664\, d_b \rho_f^{1/2} \mu_f^{1/2} L^{-1/2} V_f^{3/2} \tag{11}$$

where μ_f is the absolute viscosity of the film's boundary layer.

The friction force (per unit length) in the liquid film/air boundary layers, D_a, is estimated similarly; see also Couder et al. (1989):

$$D_a = 0.664\, b \rho_a^{1/2} \mu_a^{1/2} L^{-1/2} V_f^{3/2} \tag{12}$$

where ρ_a and μ_a are the air's density and absolute viscosity, respectively.

The ratio of the two friction forces is given by

$$D_a / D_b = (b/d_b)\,(\mu_a \rho_a / \mu_f \rho_f)^{1/2} \tag{13}$$

5 The experimental work

In order to explore the validity of the developed model of the LFT, a series of experiments was conducted using a plain horizontal frame with $b = 4$ cm, and $L = 20$ cm. The cloth ribbon glued to the entire top of this frame measured 0.025 cm by 0.320 cm when dry. The four solutions used contained $C_{1,r} = 0.625$, 1.25, 2.5 and 5.0 vol% of a commercial surfactant syrup, respectively. This means approximately 3.7–30.0 million surfactant molecules per cubic micron. The chosen concentrations represent the range for lengthy operations (at least 15 min non-stop) of the LFT: For $C_{1,r}$ less than about 0.5%, the films rupture frequently (see Sect. 6), while for $C_{1,r} > 5\%$ measurement of the film flow rates becomes rather erroneous. For each solution, five water flow rates of $q_w = 95$, 110, 126, 142 and 158 cm^3/s were used, the corresponding water sheets running at $V_w = 95$–158 cm/s. It was noted that for every solution, the liquid film becomes almost stationary when water flow rate is lowered to about 75 cm^3/s, although the film is still in contact with water. For water flow rates greater than about 160 cm^3/s the films become unstable: they vibrate too much and burst too often. It becomes very hard to produce any film when $q_w \cong 210$ cm^3/s. The water sheets measure 12.50 cm by 0.08 cm and the maximum possible q_w at present is about 230 cm^3/s.

In each case, the average film velocity was estimated by a particle tracing technique, while the average film flow rate was measured by weighing the reservoir before and after each run. They were in the range of $V_f = 8$–30 cm/s and $q_f = 0.005$–0.055 cm^3/s, respectively. The film velocities were later checked by a laser Doppler velocimeter and showed good accordance. The average film thickness, d_f, was calculated as q_f / V_f to be about 1.6–5.4 μm.

6 Results and discussion

Figure 11 shows that the film flow rates increase with increasing water sheet velocity but flat out as the latter approaches 1.6 m/s. This trend is the same as the one observed for the film velocities (Fig. 12), as expected, since the film thickness in model of Sect. 4.2 is independent of water sheet velocity. This fact is stressed further in Figs. 14 and 15, as discussed later.

The behavior of V_f (or q_f) points to a balance between the pulling force generated by the water sheet and the opposing forces of friction and the reservoir's pull (as discussed in Sect. 4.3). As water velocity is increased, the opposing forces become more significant, and, finally, there are cases where an increase in V_w does not affect V_f (or q_f). At this limiting V_w, taking the saturation V_f of 1.6 m/s as V_a, and using $E_M \cong 0.08$ N/m, Eq. (6) yields a limiting d_f of about 60 μm. In other words, it is impossible to operate the LFT with such thick films.

The LFT model postulated in Sect. 4.3 was tested using Fig. 12 at several values of V_f. To do this, several pairs of points were chosen such that each pair had the same V_f. When

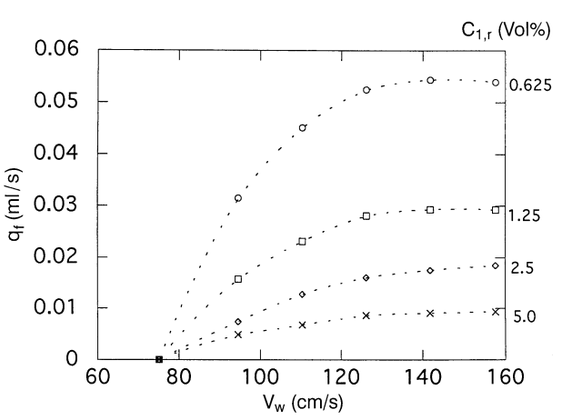

Fig. 11. Liquid film flow rate versus water sheet velocity

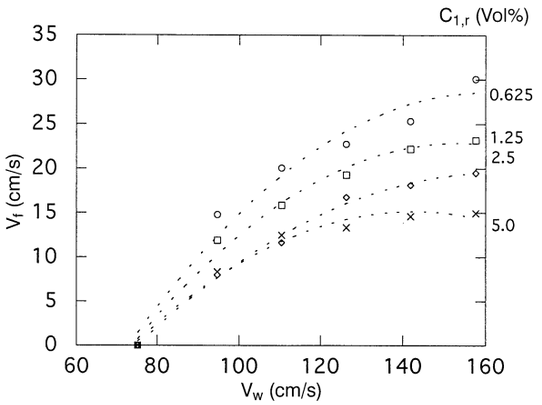

Fig. 12. Liquid film velocity versus water sheet velocity

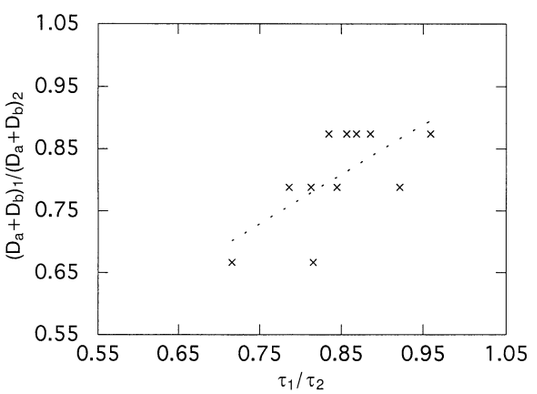

Fig. 13. Boundary layer friction force-shear stress relation

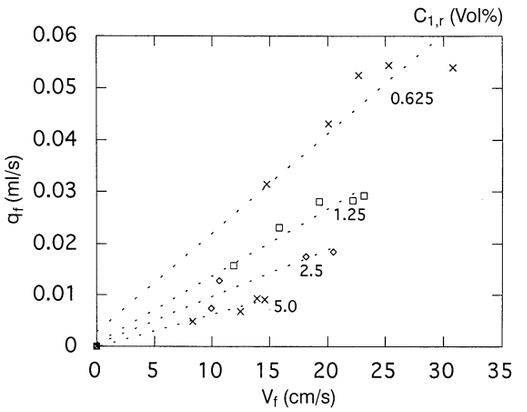

Fig. 14. Liquid film flow rate versus liquid film velocity

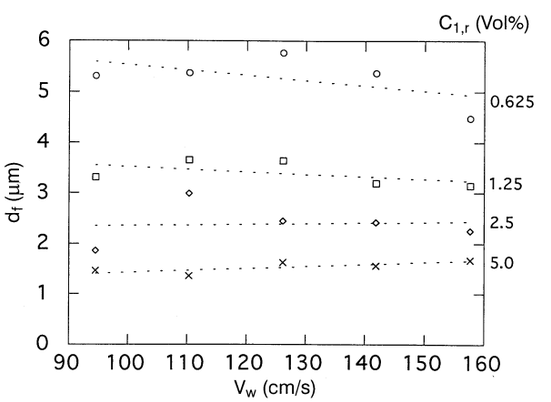

Fig. 15. Liquid film thickness versus water sheet velocity

comparing the two points 1 and 2 in any of these pairs, one has, given $(D_b)_1/(D_b)_2=[(\mu_f)_1/(\mu_f)_2]^{1/2}$ [by Eq. (11)], and employing Eq. (10), $\tau_1/\tau_2=[V_w/d_f^{1/2}]_1/[V_w/d_f^{1/2}]_2$ is approximately proportional to

$$(D_a+D_b)_1/(D_a+D_b)_2=\{[1+(D_a+D_b)_1]/[1+(D_a+D_b)_2]\}[(\mu_f)_1/(\mu_f)_2]^{1/2} \quad (14)$$

The D_a/D_b ratios were estimated by Eq. (13), with d_b taken as the thickness of the dry ribbon and μ_f estimated by Trapeznikov's (1957) method (see also, Mysels et al. 1959; Gharib and Derango 1989), using our measured (by a Cannon–Fenske tube) bulk viscosities. For the four solutions used in our experiments, i.e. with $C_{1,r}=0.625$, 1.25, 2.5 and 5.0%, the estimated values of μ_f are 3.75, 5.40, 7.06 and 10.72 cP, respectively. The corresponding D_a/D_b ratios are 0.384, 0.320, 0.280 and 0.227, respectively. Since d_b is actually larger than the dry-ribbon thickness because of meniscus formation, the real D_a/D_b ratios are even smaller than these estimated values.

The agreement between the results, as shown in Fig. 13, was observed to be fairly good. The differences arise from several facts. First, the shear-stress ratio of Eq. (14) implies that the shear area is same for points 1 and 2. This may be a good assumption, because the films containing a higher amount of surfactant should dissolve more rapidly than those with a lower amount, as required by mass-transfer laws. This may well affect the contact area, i.e. the shear area. Second, in the calculation of D_a/D_b ratios, the estimates of film's viscosity and boundary thickness were not quite accurate. Finally, the reservoir's pulling force F_o was not taken into account because it corresponds to a small film/water sheet contact area.

The relationship between q_f and V_f is examined in Fig. 14. Since the plotted data fit fairly well to straight lines, the film thickness must be independent of water sheet velocity, as in liquid film model of Sect. 4.2. To stress this further, the average film thickness, i.e., q_f/V_f, is plotted versus V_w in Fig. 15 for different supply solutions.

These results strongly support the validity of the theoretical model employed for the film, since they show that d_f is independent of V_w.

In order to find out why liquid films do not last when the supply solution is too dilute, the following calculations were performed:

$$\Gamma_1=(\sigma_o-\sigma)/RT=(44\ \text{dyn/cm})/(8.3143\times10^7\ \text{erg/K mol})\ (300\ ^\circ\text{K})$$

$$\Gamma_1=(1.764\times10^{-9}\ \text{mol/cm}^2)\ (6.022\times10^{23}\ \text{molecules/mol})$$

$$\Gamma_1=1.062\times10^{15}\ \text{molecules/cm}^2=10.62\ \text{million molecules/}\mu\text{m}^2$$

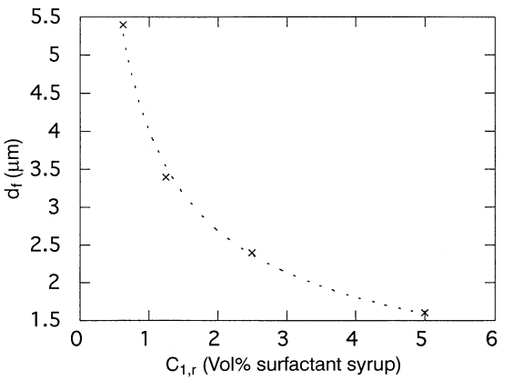

Fig. 16. Liquid film thickness versus surfactant content of supply solution

Thus, there are 9.413 Å^2/surfactant molecule. Thus is quite low, since it represents a 3.46 Å diameter circle, comparable to molecular sizes.

Using the mean film thickness (Fig. 15) and assuming $C_{1,f}=C_{1,r}$, the number of surfactant molecules per square micron of the films is calculated as shown in Table 1.

$C_{1,r}$ [%]	0.625	1.25	2.5	5.0
Mean d_f[μm]	5.4	3.4	2.4	1.6
Total molec. [millions]	19.72	25.42	35.85	46.20
Molec. in interstitial layer [millions]	Trace	4.2	14.6	25.0

Therefore, liquid films made from supply solutions more dilute than 0.625% can hardly sustain. This is because the interstitial layer not only cannot supply any surfactant molecule, but tries to rob them out of the surfaces. This explains why liquid films for $C_{1,r}<0.5\%$ pop frequently.

This conclusion becomes more emphasizing when film thickness is plotted versus supply solution's concentration; see Fig. 16.

7 Conclusions

The experimental results and the foregoing discussion clearly show that the postulated model does indeed define the physical fundamentals and operational mechanisms of the LFT. Liquid film thicknesses are governed by thermodynamic processes rather than hydrodynamics, and their elasticity is defined by Gibbs modulus except when there are rapid local disturbances, warranting a Marangoni treatment. In other words, under steady environmental conditions and using the same surfactant, a film thickness is merely determined by surfactant concentration in the supply solution.

There exists a relation between the film thickness and concentration of its supply solution, as shown in Fig. 16, which also points to limits of film thickness: For very dilute supply solutions, the films are too thick and are hard to sustain because they do not contain enough surfactant molecules. At the other limit, i.e. when the supply solutions are relatively too concentrated, film thickness gradually approaches nanometer ranges.

The fundamental physics of LFT operation is defined simply by a convenient force balance. The frictional forces of the film's boundary layers with air and ribbons plus the resistive pulling force of the reservoir's surface are overcome by a driving force originating at the film/water sheet contact. This force is produced by momentum transfer due to dissolution of the film's surfactant molecules into the water sheet. In other words, a shear stress is generated there because of the forced mass transfer from film to water sheet.

Friction due to air/film boundary layer is shown to be smaller than that of ribbon/film. The reservoir's pulling force is also small because it corresponds to a small film/water sheet contact area. Therefore, an approximate form of the force balance, as shown in Eq. (14), is employed to prove the correctness of the postulated model.

Further explanation of the forces acting on the LFT is given in the appendix.

Since the friction imparted on the film's edges by the frame structure is the dominant factor in limiting the maximum velocity of the film, it would be important that the future improvement of the LFT designs incorporate ideas that reduce this friction force.

Appendix

Explanation of forces acting on the LFT

The explanation of the forces for the horizontal design starts with F_f. Evidently, this force originates from the pulling action of the fast-moving water sheet, which has always a much lower surfactant concentration and thus a higher surface tension than the supply solution. This fact prompts the question of whether F_f is a function of surface-tension difference or concentration difference or both. In any case, what is the effect of the momentum carried by the water sheet? A third but related question concerns the role of the involved materials. In other words, we would like to know how well other liquids will pull the surfactant films.

Regarding the first question, we noted that in experiments of Sect. 5 there always exists a minimum water-sheet flow rate at which the film's movement becomes negligible, although it continues to contact the running water sheet and dissolve in it. In another experiment, the downstream side of the frame was put in a large-area container of still water, then a liquid film was formed as before. Although the film started to move, the motion was even slower than the cases with the minimum-rate water sheets, and eventually ceased as the water surface was covered by surfactant molecules.

Since the surface tension of the four solutions used in the experiments of Sect. 5 is the same, i.e., 28.0 dyn/cm (Fig. 17), and their densities are very close to that of water, another experiment was conducted as follows. Using the 0.625% supply solution and the 142 cm^3/s water-sheet rate, some surfactant was added to the water supply tank in several steps until the water sheet contained 5% surfactant syrup. At each step, the film flow rate and velocity was measured as before. The results,

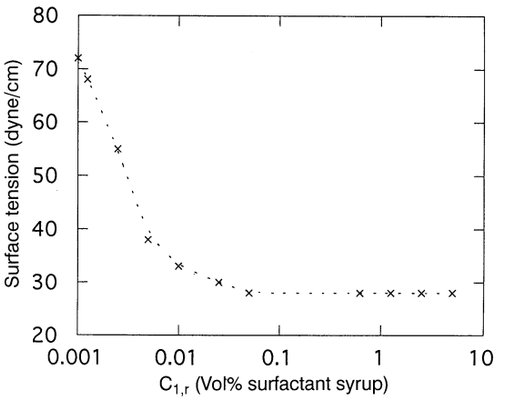

Fig. 17. Surface tension of the supply solutions

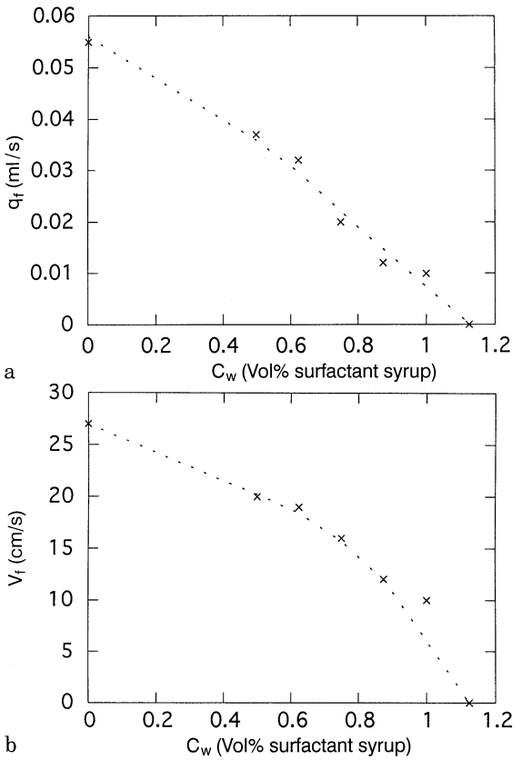

Fig. 18. a Liquid film flow rate versus surfactant content of the water sheet for $C_{1,r}=0.625\%$ and $q_w=142\,\mathrm{cm^3/s}$; **b** liquid film velocity versus surfactant content of the water sheet for $C_{1,r}=0.625\%$ and $q_w=142\,\mathrm{cm^3/s}$

as shown in Figs. 18a, b, indicate that both flow rate q_f and velocity V_f of the liquid films decrease as the surfactant content of the water sheet, C_w, is increased. Finally, the films cease to move when C_w is greater than about 1.125%.

From these experiments we learn that surface-tension difference is not directly responsible for the motion of the surfactant films. Rather, a film moves because its downstream part is washed away by the water sheet and it tries to re-form by pulling more surfactant from the reservoir upstream. This re-formation becomes possible since a surfactant film is an elastic material. The surface-tension difference enters the picture through the governing equation of state [Eq. (3)]. Note that an efficient dissolution of the film requires a fast-moving water sheet, since the mass diffusivity of surfactants in water is relatively small. This explains why the experiments with the minimum-rate water sheet and the one with still water produced negligible film flows.

The answer to the second question is evident now. The momentum carried by the water-sheet increases the surfactant dissolution rate because it enhances mixing. This effect is even stronger when the water sheet is more concentrated than the film, so it cannot dissolve the film by mass diffusion. This explains why the films will flow even under these negative concentration gradients, which, naturally oppose the film dissolution (see Figs. 18a and b). In other words, as the water-sheet concentration is increased, the dissolution rate, and thus the film flow, decreases until we reach to a point when no more dissolution occurs.

In order to answer the third question, we conducted several other experiments, in which we tried to run the films by means other than water. Kerosene did not grab the film at all, while ethanol and acetone burst them instantly, upon contact. For these liquids, the surface tension at room temperature is in the range of 20–30 dyn/cm. Suction by vacuum also popped the films instantly.

These preliminary experiments suggest that a measurable motion does not occur unless the pulling medium can dissolve the liquid film at a considerable rate. In other words, as the surfactant molecules are washed away downstream, the liquid film supplies fresh molecules by pulling them out of the reservoir. This phenomenon is fully expected, since surfactant films are elastic media in essence.

The aforementioned experimental evidences led to the following postulation for explaining the source and nature of the external force F_f. As the upper surface of the water sheet touches the lower surface of the liquid film, the surfactant molecules, which populate the latter, start migrating to the former due to chemical potential difference. Since the three layers of the liquid film move together and their thermodynamic equilibrium is disturbed by the mentioned contact, their elastic reaction leads to pulling more surfactant molecules from the neighboring section of the film. This section, in turn, pulls more molecules from the other sections further upstream, and finally, the reservoir. In this manner, a shear force $F_f=\tau A_c$ is generated at the film/sheet contact area of A_c.

A question that comes up here is whether the force generated at the film/water sheet contact due to surface tension difference (between film and sheet) is comparable to the shear force envisioned in the LFT model. To answer this, recall that for every surfactant concentration in Sect. 5 $(\sigma_o-\sigma)=72-28=44$ dyn/cm. Given $b=4$ cm, this means $2\times44\times4=352$ dyn for the sum of upper and lower contact lines. On the other hand, Eq. (10) gives a minimum of about 14400 dyn when $V_w=75$ cm/s, $d_f=5.4\,\mu$m, $V_a=600$ cm/s (Couder et al. 1989) and $A_{c,\min}=0.32\,\mathrm{cm^2}$, the cross-sectional contact area of the water sheet. Note that since the contact is tangential, the shear area is actually much more than $0.32\,\mathrm{cm^2}$, and thus F_f is much higher than 14400 dyn. Also note that this minimum

force is equal to F_o for a film from a 0.625% solution, because there is no film motion and thus no boundary-layer friction.

References

Beizaie M (1991) Physical fundamentals of the surfactant film tunnel. Bull Am Phys Soc 36: 2718

Bluestein BR; Hilton CL (1982) Amphoteric surfactants, pp 5, 178, 268. New York: Marcel Dekker

Chirash W (1981) Liquid light-duty detergents. J Am Oil Chemists Soc 58: 362A–366A

Couder Y (1981) The observation of a shear flow instability in a rotating system with a soap membrane. J Phys Lett 42: L429–31

Couder Y; Chomaz JM; Rabaud M (1989) On the hydrodynamics of soap films. Physica D 37: 384–405

Cross J (1977) Nonionic surfactants-chemical analysis, pp 4. New York: Marcel Dekker

Frankel S; Mysels KJ (1969) The bursting of soap films, II, theoretical considerations. J Phys Chem 73: 3028–3038

Gharib M (1993) Studies of two-dimensional flows via soap-films. Bull Am Phys Soc 38: 2308

Gharib M; Beizaie M (1989) Studies of incompressible and compressible 2-D laminar and turbulent jets via soap-film tunnel. Bull Am Phys Soc 34: 2326

Gharib M; Beizaie M (1990) Studies of two-dimensional grid turbulence via soap-film tunnel. Bull Am Phys Soc 35: 2296

Gharib M; Beizaie M (1992) A novel soap-film tunnel for studying two-dimensional flows. In: Flow visualization VI, Proc 6th Int Symp Flow Visualization, eds., Y Tanida; H Miyashiro, pp 233–237. New York: Springer

Gharib M; Derango P (1987) Development of a soap-film tunnel to study two-dimensional laminar shear flows. Bull Am Phys Soc 32: 2031

Gharib M; Derango P (1989) A liquid film (soap film) tunnel to study two-dimensional laminar and turbulent shear flows. Physica D 37: 406–416

Isenberg C (1978) The science of soap films and soap bubbles. Clevedon, UK: Tieto

Liepmann HW; Roshko A (1957) Elements of gasdynamics. New York: Wiley

Mysels KJ; Frankel S (1978) The effect of a surface-induced gradual viscosity increase upon the thickness of entrained liquid films and the flow in narrow channels. J Colloid Interf Sci 66: 166–172

Mysels KJ; Shinoda K; Frankel S (1959) Soap films: studies of their thinning and a bibliography. New York: Pergamon

Roshko A (1953) On the fundamental of turbulent wakes from vortex stretching, NACA TN: 2913

Rusanov AI; Krotov VV (1979) Gibbs elasticity of liquid films, threads, and foams. Progr Surf Membrane Sci 13: 415–524

Schick MJ (1987) Nonionic surfactants-physical chemistry, p 821. New York: Marcel Dekker

Schlichting H (1968) Boundary layer theory. Oxford: Pergamon

Trapeznikov AA (1957) application of the method of two-dimensional viscosity and shear strength to the investigation of the structure and composition of two-sided films and surface layers in solutions of soaps and saponins. Proc 2nd Int Cong on Surface Activity, ed J.H. Shulman, pp 242–258, London: Butterworths